INRIA

INSTITUT NATIONAL DE RECHERCHE EN INFORMATIQUE ET EN AUTOMATIQUE

# *A Critical Evaluation of the Classical $k-\varepsilon$ Model and Wall-Laws for Unsteady Flows over Bluff Bodies*

Bijan Mohammadi and Gorazd Medic

**N° 3056**

Decembre 1996

THÈME 4


ISSN 0249-6399

INRIA
ROCQUENCOURT

# A Critical Evaluation of the Classical $k-\varepsilon$ Model and Wall-Laws for Unsteady Flows over Bluff Bodies

Bijan Mohammadi *and Gorazd Medic †

Thème 4 — Simulation et optimisation
de systèmes complexes

Projet M3N

Rapport de recherche n°3056 — Decembre 1996 — 27 pages

**Abstract:** The classical $k-\varepsilon$ model and a new implementation of wall-laws have been evaluated for unsteady turbulent flows past square and circular cylinders. We show that good numerics can lead to a serious improvement of the results. In the case of the flow past a square cylinder (Lyn's test case), results agree surprisingly well with the experimental data. In the analysis of the vortex shedding flow past a circular cylinder also the agreement is quite good for the sub-critical regime but not entirely satisfactory after the critical Reynolds number (i.e. the drag crisis phenomenon).

**Key-words:** turbulence, unsteady, $k-\varepsilon$, wall-laws

*(Résumé : tsvp)*

* e-mail: Bijan.Mohammadi@inria.fr
† e-mail: Medic.Gorazd@inria.fr

Unité de recherche INRIA Rocquencourt
Domaine de Voluceau, Rocquencourt, BP 105, 78153 LE CHESNAY Cedex (France)
Téléphone : (33 1) 39 63 55 11 – Télécopie : (33 1) 39 63 53 30

# Evaluation critique du modèle $k-\varepsilon$ classique et les fonctions de paroi pour les écoulements instationnaire autour de corps complexes

**Résumé :** On présente l'étude du modèle $k-\varepsilon$ classique et des nouvelles lois de paroi pour des écoulements instationnaires turbulents autour de cylindres à sections carrée et circulaire. Nous montrons qu'une bonne méthode numérique conduit à de très bons résultats. Pour la première configuration (cas-test de Lyn), nous remarquons une bonne correlation avec léxpérience. Pour le cylindre circulaire les résultats sont satisfaisants pour le régime sous-critique tandis que des lacunes apparaissenet après la crise de la trainée.

**Mots-clé :** turbulence, instationnaire, $k-\varepsilon$, loi de paroi

# Contents

# 1 Introduction

It is usually stated that the standard $k-\varepsilon$ model even including a low-Reynolds modeling can not predict the details of an unsteady flow such as the flow over square or circular cylinders. In this paper, the standard $k-\varepsilon$ model and wall-laws are used for such a computations and it is shown that our wall-laws implementation based on four ingredients leads to very good results. These ingredients are:
1. global wall-laws (i.e. valid $\forall y^+$),
2. use of weak formulation,
3. use of small $\delta$ in wall-laws (to keep the computational domain not too far from the wall),
4. use of reasonably fine meshes.

As this paper is about the impact of the numerics on the results, the influence of the following implementation details has also been analyzed:
1. use of different wall-laws (logarithmic wall function, Reichardt wall function, Reichardt wall function with convection and pressure gradient correction and the combination of wall-laws with two-layer technique),
2. the mesh dependency of the solution, and in particular the influence of mesh refinement near walls,
3. the influence of the artificial dissipation.

Results have been compared with available experimental data and other computations (using LES, RSE or other $k-\varepsilon$). In particular, we use the review paper of Rodi [14] for these problems. Our results are comparable with the best results available in the literature for the Lyn's configuration but not entirely satisfactory for the circular cylinder above the critical Reynolds number. This is not surprising as the flow has a three dimensional feature then.

# 2 Model and Numerics

## 2.1 Mathematical model

We split the variables into mean and fluctuating parts. We use the Reynolds average for the density and pressure and the Favre average for the other variables. We then consider the Reynolds averaged Navier-Stokes equations. Once the unknown correlations are modeled [2], we have:

$$\frac{\partial \rho}{\partial t} + \nabla \cdot (\rho u) = 0$$

$$\frac{\partial \rho u}{\partial t} + \nabla \cdot (\rho u \otimes u) + \nabla p = \nabla \cdot ((\mu + \mu_t) S) \tag{1}$$

$$\frac{\partial \rho E}{\partial t} + \nabla \cdot ((\rho E + p) u) = \nabla \cdot ((\mu + \mu_t) S u) + \nabla((\kappa + \kappa_t)\nabla T)$$

with

$$\kappa = \frac{\gamma \mu}{Pr}, \quad \kappa_t = \frac{\gamma \mu_t}{Pr_t},$$

$$\gamma = 1.4, \quad Pr = 0.72 \quad \text{and} \quad Pr_t = 0.9,$$

Where $\mu$ and $\mu_t$ are the inverse of the laminar and turbulent Reynolds numbers. In what follows, we call them viscosity. The laminar viscosity $\mu$ is given by Sutherland law but this is not very important for the cases presented here:

$$\mu = \mu_\infty (\frac{T}{T_\infty})^{1.5} (\frac{T_\infty + 110.}{T + 110.}), \tag{2}$$

where $\infty$ denotes reference quantities.

We do not take into account the turbulent kinetic energy contribution to the pressure and total energy and keep the usual laws for perfect gas.

The $k - \varepsilon$ model [1] we use is classical and is an extension to compressible flows of its incompressible version [2] and is defined by:

$$\frac{\partial \rho k}{\partial t} + \nabla.(\rho u k) - \nabla((\mu + \mu_t)\nabla k) = S_k, \tag{3}$$

and

$$\frac{\partial \rho \varepsilon}{\partial t} + \nabla.(\rho u \varepsilon) - \nabla((\mu + c_\varepsilon \mu_t)\nabla \varepsilon) = S_\varepsilon. \tag{4}$$

The right hand sides of (3)-(4) contain the production and the destruction terms for $\rho k$ and $\rho \varepsilon$:

$$S_k = \mu_t P - \frac{2}{3}\rho k \nabla.u - \rho \varepsilon, \tag{5}$$

$$S_\varepsilon = c_1 \rho k P - \frac{2c_1}{3c_\mu}\rho\varepsilon\nabla.u - c_2\rho\frac{\varepsilon^2}{k}. \tag{6}$$

The eddy viscosity is given by:

$$\mu_t = c_\mu \rho \frac{k^2}{\varepsilon}. \tag{7}$$

The constants $c_\mu, c_1, c_2, c_\varepsilon$ are respectively $0.09, 0.1296, 11/6, 1/1.4245$ and $P = S : \nabla u$. The constant $c_2$ and $c_\varepsilon$ are different from their original values of 1.92 and $1/1.3$.

The $c_2$ constant comes from the behaviour of $k$ in isotropic turbulence:

$$k = k_0(1 + (c_2 - 1)\frac{\varepsilon_0}{k_0}t)^{\frac{-1}{c_2-1}},$$

which is consistent with the experimental results of Comte-Bellot [5] giving a decay of $k$ in $t^{-1.2}$ if and only if $c_2 = 11/6$ while $c_2 = 1.92$ leads to a decay in $t^{-1.087}$ and therefore to an overestimation of $k$. This has also been reported in [6], where the author managed to compute the right recirculating bubble length for the backward step problem using the standard $k-\varepsilon$ model with $c_2 = 11/6$ and wall-laws but with $c_\varepsilon = 1/1.3$. In this work we have used the compatibility relation between the $k-\varepsilon$ constants to deduce $c_\varepsilon$:

$$c_\varepsilon = \frac{1}{\kappa^2\sqrt{c_\mu}}(c_2 c_\mu - c_1), \quad \kappa = 0.41,$$

which comes from the requirement of a logarithmic velocity profile in the boundary layer.

## 2.2 Numerics

Spatial discretization of the Navier-Stokes equations is based on a Finite-Volume-Galerkin formulation. In this paper we use a Roe [7] Riemann solver for the convective part of the equations together with MUSCL reconstruction with Van Albada [8] type limitors. However, the limitors are only used in presence of shocks. The viscous terms are treated using a Galerkin Finite Element method on linear triangular elements.

We give a brief description of this technique applied to 1. Consider the following form of the Navier-Stokes equations:

$$\frac{\partial W}{\partial t} + \nabla.(F(W) - N(W)) = 0, \tag{8}$$

where $W = (\rho, \rho u, \rho v, \rho E)^t$ is the vector of conservation variables, $F$ and $N$ are the convective and diffusive operators.

Let $\Omega_h = \cup_j T_j$ be a discretization by triangles of the computational domain $\Omega$ and let $\Omega_h = \cup_i C_i$ be its partition in cells.

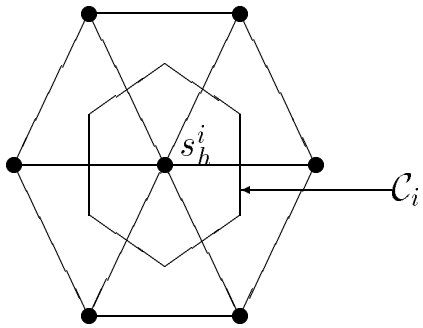


Thus, we can associate to each $w_h \in V_h$, where $V_h$ is the set of the continuous affine functions on our triangulation, a $w_h'$ piecewise constant function on cells by

$$w_h'|C_i = \frac{1}{|C_i|}\int_{C_i} w_h.$$

Conversely, knowing $w_h'$ piecewise constant, $w_h$ is obtained as $w_h(S_i) = w_h'|C_i$.

The weak formulation of (8) is:

Find $W_h \in (V_h)^6$ such that, $\forall \phi_h \in V_h$

$$\int_\Omega \frac{\partial W_h}{\partial t}\phi_h - \int_\Omega (F_h - N_h)(W_h)\nabla(\phi_h) \tag{9}$$

$$+ \int_{\partial\Omega} (F_h - N_h)\cdot n\phi_h = 0.$$

This is equivalent to the following weak formulation obtained by taking in the convective part of (9) for $\phi_h$ the characteristic function of $C_i$ and by using an explicit time integration:

$$|C_i|(\frac{W_i^{n+1} - W_i^n}{\Delta t}) + \int_{\partial C_i} F_d(W^n)\cdot n = R.H.S. \tag{10}$$

We use a centered scheme to compute the right hand side:

$$R.H.S. = -\int_{\Omega_h} N(W^n)\nabla(\phi_h) + \int_{\partial\Omega} N(W^n)\cdot n\phi_h.$$

Moreover, $F_d(W_h^n) = F(W_{\partial\Omega})$ on $\partial C_i \cap \partial\Omega$ and elsewhere $F_d$ is a piecewise constant upwinded approximation of $F(W)$ satisfying

$$\int_{\partial C_i} F_d \cdot n = \sum_{j \neq i} \Phi(W'|_{C_i}, W'|_{C_j}) \int_{\partial C_i \cap C_j} n. \tag{11}$$

After, writing $\tilde{B}$ for the jacobian of $F$ at Roe's mean values, we take for $\Phi$ the Roe flux

$$\Phi_{Roe}(u,v) = \frac{1}{2}(F(u) + F(v)) - |\tilde{B}|\frac{(v-u)}{2}.$$

Spatial second order accuracy is obtained by using a MUSCL like extension involving a combinations of upwind and centered gradients. More precisely, let $\nabla W_i$ be an approximation of the gradient of $W$ at node i. We define the following quantities on the segment $[i,j]$

$$W_{ij} = W_i + 0.5\mathrm{Lim}(\beta(\nabla W)_i \vec{ij}, (1-\beta)(W_i - W_j)),$$

and

$$W_{ji} = W_j - 0.5\mathrm{Lim}(\beta(\nabla W)_j \vec{ij}, (1-\beta)(W_j - W_i),$$

with Lim being a Van Albada type limitor [7]:

$$\mathrm{Lim}(a,b) = 0.5(1 + sgn(ab))\frac{(a^2+\alpha)b + (b^2+\alpha)a}{a^2+b^2+2\alpha}$$

with $0 < \alpha << 1$ and $\beta$ a positive constant containing the amount of upwinding $\beta \in [0,1]$ (here $\beta = 2/3$). Now, the second order accuracy in space is obtained by replacing $W_i'$ and $W_j'$ in (11) by $W_{ij}$ and $W_{ji}$. These techniques have been successfuly extended to unstructured meshes in the past [9].

However, the limitors presented above were not used in the computations presented in this analysis.

This approach does not guarantee the positivity of $\rho k$ and $\rho\varepsilon$. Therefore, the convective fluxes for the turbulent equations are computed using the PSI fluctuation splitting scheme [10] which is positive and linear preserving.

The boundary and initial conditions are classical. In particular, a Stegger-Warming [11] flux splitting scheme is used for in and outflow boundaries.

The spatial discretization (10) has been presented together with a first order scheme in time but as we are targeting unsteady computations, it is important to have a precise time integration scheme. In this paper, a low-storage four steps Runge-Kutta scheme has been used. Lets rewrite (8) as

$$\frac{\partial W}{\partial t} = RHS(W),$$

where $RHS$ contains the nonlinear operators. The Runge-Kutta scheme we use is given by:

$$W^0 = W^n$$

$$W^k = W^0 + \alpha_k \Delta t RHS(W^{k-1}) \quad \text{for} \quad k = 1, .., 4$$

$$W^{n+1} = W^4$$

with the following choices [12] for $\alpha_k$:

$$\alpha_1 = 0.11, \alpha_2 = 0.2766, \alpha_3 = 0.5, \alpha_4 = 1.0.$$

This scheme has been detailly studied in [12].

## 2.3 The implementation of wall-laws

In weak form (finite element or finite volume approach) the following boundary integral appears in the momentum equation ( $(\vec{s}, \vec{n})$ denotes the local orthogonal basis for a wall node):

$$\int_{\Gamma_w} (\mathbf{S}.\vec{n}) d\sigma,$$

where $\mathbf{S} = (\nu + \nu_t)(\nabla u + \nabla u^t)$ is the Newtonian strain tensor. We decompose $\mathbf{S}.\vec{n}$ over $(\vec{s}, \vec{n})$:

$$\mathbf{S}.\vec{n} = (\mathbf{S}.\vec{n}.\vec{n})\vec{n} + (\mathbf{S}.\vec{n}.\vec{s}).\vec{s}. \tag{12}$$

In our implementation, the first term $(S_{nn})$ in the right hand side of (12) is computed explicitly. It becomes important for the separation and reattachement points, but from numerical point of view, it decreases the robustness of the flow solver, and was therefore neglected in the presented computations. Furthermore, the following wall-laws are used:

$$\vec{u}.\vec{n} = 0,$$

$$(\mathbf{S}\vec{n}.\vec{s})\vec{s} = -u_\tau^2 \vec{s},$$

where $u_\tau$ is the friction velocity, solution of $\vec{u}.\vec{s} = u_\tau f(u_\tau)$. We decompose $f(u_\tau)$ in two parts:

$$f(u_\tau) = f_r(u_\tau) + f_c(u_\tau),$$

with $f_r(u_\tau)$ the nonlinear Reichardt equation:

$$f_r(y^+) = 2.5log(1 + \kappa y^+) + 7.8(1 - e^{-y^+/11} - \frac{y^+}{11} e^{-0.33y^+}),$$

with $y^+ = \frac{u_\tau y}{\nu}$ and with $f_c$ a new contribution when pressure and convection effects exist:

$$C = \frac{\partial p}{\partial s} + u\frac{\partial u}{\partial s} + v\frac{\partial u}{\partial n}.$$

In this case, $f_c$ is given by:

$$f_c(y^+) = (\frac{35C\nu}{\kappa u_\tau^3})\log(1+\kappa\frac{(y^+)^2}{70}) \quad \text{if} \quad y^+ \leq 5.26, \tag{13}$$

and

$$f_c(y^+) = \frac{C\delta}{\kappa u_\tau^2}, \quad \text{if} \quad y^+ \geq 5.26. \tag{14}$$

Of course, this correction vanishes with $C$ and we recover the Reichardt law. This additional convection and pressure gradient correction $f_c(u_\tau)$ has been validated and successfully used for the backward facing step computation in [3] predicting a main recirculation of length 7 and a secondary bubble of length and height of about 0.2 and 0.3.

Once $u_\tau$ is computed, $k$ and $\varepsilon$ are set to:

$$k = \frac{u_\tau^2}{\sqrt{c_\mu}}\alpha, \quad \varepsilon = \frac{u_\tau^3}{\kappa\delta}min(1, \alpha + \frac{0.2\kappa(1-\alpha)^2}{\sqrt{c_\mu}}),$$

where $\delta$ is the distance of the fictitious computational domain from the solid wall and $\alpha = min(1, \frac{y^+}{10})$ reproduces the behavior of $k$ when $\delta$ tends to zero. The distance $\delta$ is given a priori and is kept constant during the computation. As we said, $\delta$ is choose-d such that $y^+$ remains small (less than 100). But, therefore, in regions where $y^+$ is small, the standard $k-\varepsilon$ model is no longer valid. To see the influence of this on the results, we use a modified two-layer $k-\varepsilon$ model [2, 4] coupled with the previous wall-laws as follows:

For internal mesh nodes where $y^+ < 200$, the $\varepsilon$ equation and the eddy viscosity expression are respectively replaced by the following algebraic expressions:

$$\varepsilon = \frac{k^{\frac{3}{2}}}{l_\varepsilon}, \quad \nu_t = c_\mu\sqrt{k}l_\mu$$

and $l_\varepsilon$ and $l_\mu$ are two length scales containing the damping effects in the near wall regions.

$$l_\mu = \kappa c_\mu^{-3/4} y(1 - e^{(\frac{-y^+}{c})}),$$

$$l_\varepsilon = \kappa c_\mu^{-3/4} y(1 - e^{(\frac{-y^+}{2\kappa c_\mu^{-3/4}})})$$

where $c = 70$ and $\kappa = 0.41$ and $y^+$ is defined as

$$y^+ = \frac{\sqrt{k}y}{\nu},$$

where $y$ is the distance of the current point to the wall (i.e. distance to the fictitious boundary plus $\delta$).

# 3 Numerical results

In this section we present numerical results for two test cases of unsteady flows past cylinders. These results are compared with experimental data and also with other existing simulations based on various approach ranging from eddy viscosity and Reynolds stress models to LES.

As the purpose of this analysis is to analyze the behavior of the standard $k-\varepsilon$ model with wall laws, and its competitiveness with other turbulence modeling approaches for this test case, special attention was payed on the impact of different implementation factors (mesh refinement, additional two layer technique and spatial accuracy) on both the global (integral) parameters of the flow and the detailed distribution of field values in the vicinity of cylinders.

All these computations have been done using NSC2KE flow solver [4] which is in free access (anonymous ftp on piranha.inria.fr under pub/) on a HP workstation making 10 MFlops.

## 3.1 Flow past a square cylinder

This is the Lyn's vortex shedding past a square cylinder test case at $Re_{\infty/D} = 22000$. Detailed experimental results obtained by Lyn's LDA measurements and a variety of simulation results using different models can be found in [13, 14, 15].

Franke and Rodi [16] performed computations using the Reynolds averaged Navier-Stokes equations, with both the $k-\varepsilon$ and the Reynolds-stress equations models (the standard RSE model of Launder, Reece and Rodi with wall corrections for the pressure-strain term due to Gibson and Launder). In both cases they tested the use of wall functions and the two-layer approach for the treatment of the near-wall regions. Murakami et al [14] employed the standard Smagorinsky model in their LES computations where the near-wall region, due to very small scales of motion contributing to the turbulent momentum transfer, was not resolved. It was rather modeled using a relation between the wall shear stress and the velocity at the first grid-point away from the wall. Haroutunian and Engelman's [13] computations is based for the high-Reynolds region on the standard $k-\varepsilon$ model or the extended $k-\varepsilon$ model of Chen and Kim, (with the additional source term $c_3\frac{k^3}{\varepsilon^2}P^2$ in the dissipation equation and different values for model constants) or an RNG $k-\varepsilon$ model. While they used a two-layer model for the low-Reynolds regions.

The main feature of the flow (i.e.the periodic shedding) is in general well predicted with most of the models and numerical methods used so far. Although, Rodi [14] reports that Franke and Rodi's calculations [16] with the standard $k-\varepsilon$ model and wall functions remained steady. Nevertheless, Rodi [14] also reports that the same

calculations [17] with a newly developed code that uses non-staggered grids (the first calculations were performed on staggered grids) yield to sustained vortex-shedding. However, so far, no single calculation was entirely satisfactory.

Until now the results obtained with the standard $k-\varepsilon$ model were always reported as being worse than the ones obtained with the Reynolds stress equations models and especially the ones obtained with large eddy simulations. Our aim is to show that in these results the use of inadequate near-wall models and over-diffusive numerical schemes obscured the true performance of the $k-\varepsilon$ model.

In [13] the authors have shown that by using anti-diffusive terms in the standard $k-\varepsilon$ model and changing the constants, a serious improvement can be obtained for this case. Here, we would like to avoid the introduction of any anti-diffusive term or any particular tuning of the constants.

The computations were carried out on a mesh having about 7000 nodes. The mesh is unstructured but symmetric in y. No perturbation has been introduced for getting the unsteadiness. The parameter $\delta$ is set to $5.10^{-3}D$ which corresponds to a $y^+$ of less than 50.

The integral parameters, the dimensionless shedding frequency (Strouhal number $St = f\frac{D}{U_\infty}$), the time-mean drag coefficient $\bar{c}_D$, the amplitudes of the oscillations in drag coefficient $\tilde{c}_D$ and lift coefficient $\tilde{c}_L$ obtained in the Franke and Rodi's calculations [16] with the $k-\varepsilon$ model and the Reynolds stress equations model, Murakami et al's LES calculations and Haroutunian and Engelman [13] calculations with different variants of the $k-\varepsilon$ model, and the results obtained in the present analysis are compared in Table 1.

| | $St$ | $\bar{c}_D$ | $\tilde{c}_D$ | $\tilde{c}_L$ |
|---|---|---|---|---|
| two-layer $k-\varepsilon$ [16] | 0.124 | 1.79 | 0.0 | 0.323 |
| RSE with wall functions [16] | 0.136 | 2.15 | 0.383 | 2.11 |
| two layer RSE [16] | 0.159 | 2.43 | 0.079 | 1.84 |
| LES (Murakami et al.) [14] | 0.132 | 2.10 | 0.12 | 1.58 |
| extended $k-\varepsilon$ [13] | 0.131 | 2.56 | | |
| RNG $k-\varepsilon$ [13] | 0.133 | 2.38 | | |
| experiments [14] | 0.135<br>0.139 | 2.05 -<br>2.39 | | |
| present analysis | | | | |
| $k-\varepsilon$ with wall functions | 0.138 | 2.10 | 0.17 | 1.9 |
| $k-\varepsilon$ with wall functions + two layer technique | 0.133 | 1.88 | 0.14 | 1.43 |

Table 1. Integral parameters.

We can see that LES [14] and RSE [16] computations produce quite different results. LES results seem to be the best, giving the Strouhal number value $St$ and the time mean drag coefficient $\bar{c}_D$ in very good agreement with the experimental data. The computations using RSE model with wall functions seem to produce better results for these integral parameters than the computations with the same model using the two-layer technique. On the other hand, the results obtained with various variants of the $k-\varepsilon$ model by Haroutunian and Engelman [13], indicate that these computations produce too high values for the time mean drag coefficient $\bar{c}_D$. The same authors [13] have also carried an analysis with the standard $k-\varepsilon$ model obtaining too diffusive results in general, with a Strouhal number of $St = 0.128$ and time mean drag coefficient of $\bar{c}_D = 1.68$.

The results of the present analysis, especially the ones obtained with the $k-\varepsilon$ model and wall functions, seem to agree with experimental data just as well as the LES results, although the value of Strouhal number is slightly over-predicted. We can see that the influence of the additional two-layer correction is not clear. The same computation using limiters in the spatial discretization, leading to a lower accurate scheme, gives the more smoothed results ($\bar{c}_D = 1.85$, $\tilde{c}_D = 0.1$ and $\tilde{c}_L = 1.24$). This is presented to illustrate how important is the influence of the numerical spatial scheme accuracy (artificial dissipation) on the solution for unsteady flow simulations.

Using mesh refinement in the near-wall region (about 8000 nodes) lead to a insignificant modification of all these values for the non-limited computation, showing that the chosen starting mesh is enough fine for the given value of $\delta$. Furthermore, comparison of the results obtained with different wall functions (Reichardt wall function, Reichardt wall function with convection and pressure gradient corrections) for this test case show that in this case they have not such a significant influence on the solution. However, this was expected, as in this case the main separation points are defined by the geometry.

The pressure distribution on the cylinder surface obtained with different computations and measurements (Bearman et al and Otsuki et al, see [14]), at slightly higher Reynolds number, is presented in Figure 1. At the base wall (CD in Fig. 1), the obtained results seem to agree very well with the measured $c_p$ value of about -1.4. Similar results were obtained using LES by Murakami et al [14], but the RSE and two-layer $k-\varepsilon$ model computations carried out by Franke and Rodi [16] over and under-predicted the values of $c_p$. In the stagnation approaching flow region (AB) there is a fairly good agreement between all the computations and measurements. However, along the side walls of the cylinder (BC) the difference between all the computations and measurements is more significant. The results obtained in the present analysis agrees with the experiments slightly better than the other results.

The distribution of the time-mean horizontal velocity component $\bar{u}$ along the centerline, giving the information on the time-averaged separation zone behind the

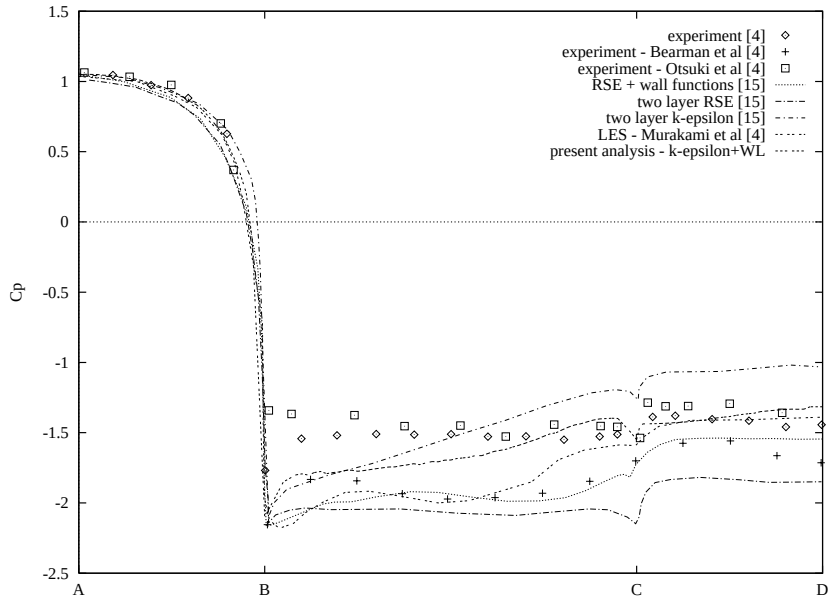


Figure 1: Pressure distribution along the surface of the cylinder.

cylinder, is presented in Figure 2. Experimental data from Lyn and Durao et al (see [14]) and the results of other simulations are also included. As for the LES and RSE computations, the present results under-predict the length of the separation zone and give poor agreement with the experiments in the free-stream velocity approaching region. But, in this region, the experimental data of Durao and Lyn are significantly different from each other. This leaves the free-stream velocity approaching mechanism somehow unclear. In all case, the present results are significantly better than the two-layer computations carried out by Franke and Rodi [16]. The results obtained with the simple Baldwin-Lomax model by Deng et al [14] have also been included, and it seems that their agreement with the experiments is the best, but it must be emphasized that there are no other results obtained with this model available.

The streamlines obtained by the RSE model using wall functions [16], LES computations (Murakamai et al) and the experimentally determined ones [14] for two of the phases are compared with the results obtained with the present approach using our wall-laws alone and coupled with the two-layer technique (Figure 3). The agreement between the results obtained with the standard $k-\varepsilon$ model with the measurements and the results obtained with RSE and LES computations is surprisingly good.

The corresponding $k$-contours are presented in Figure 4. It can be seen that the standard $k-\varepsilon$ model used in this analysis and the two-layer RSE model [16] produce similar results. However, both these results are in a significant disagreement with the experiments and LES results concerning the location of the maxima of $< k >$.

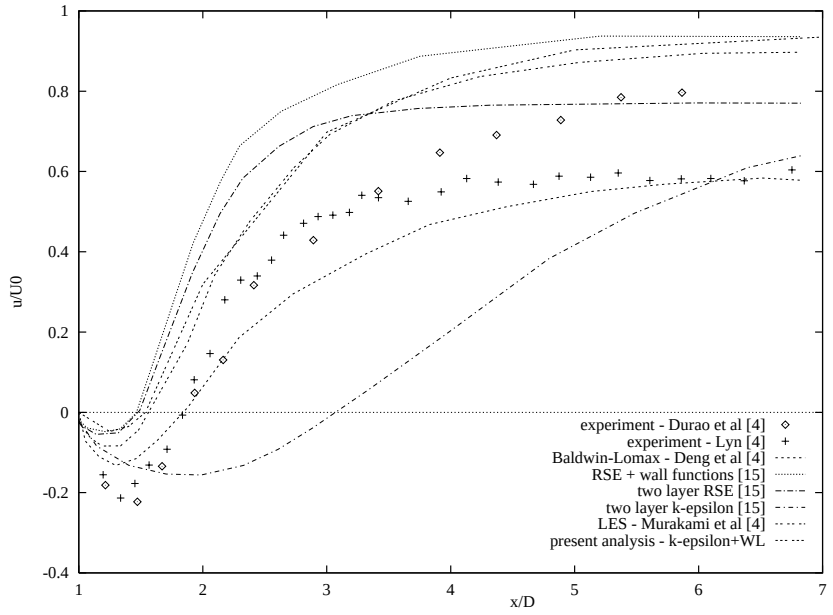


Figure 2: Time mean horizontal velocity component $\bar{u}$ along the center line.

The details of the flow in the vicinity and in the wake of the cylinder can be analyzed through figures 5, 6 and 7 where the mean horizontal velocity $< u >$ distribution along $x = D/2$ (x-position of the rear cylinder wall) and the mean lateral velocity $< v >$ variation along the centerline for phases 1 and 9 are given.

Considering the mean horizontal velocity component $< u >$ distribution, it must be emphasized that none of the computations presented in [14] has given negative velocities at the same time on both horizontal walls for the two phases considered, while the experimental data shows that the velocity near the horizontal walls is always negative at this location. However, the results obtained in the present analysis with the $k - \varepsilon$ model and global wall-laws are the closest ones to the experimental data.

The mean lateral velocity $< v >$ variation along the centerline for phases 1 and 9 (figures 6 and 7) shows that the results obtained with the $k - \varepsilon$ model are significantly better than any other result with the $k - \varepsilon$ model. Furthermore, the results obtained in this analysis with both, the $k - \varepsilon$ model with wall-laws and the $k - \varepsilon$ model with wall-laws plus the two-layer technique seem to agree with the experimental data in a similar way than in RSE and LES computations.

Concerning our two-layer correction, we conclude that its influence over the results remains unclear. In the sense that they are sometime better and sometime worse than using the original model. Therefore, for the next test case, we only use the classical $k - \varepsilon$ model and wall-laws.

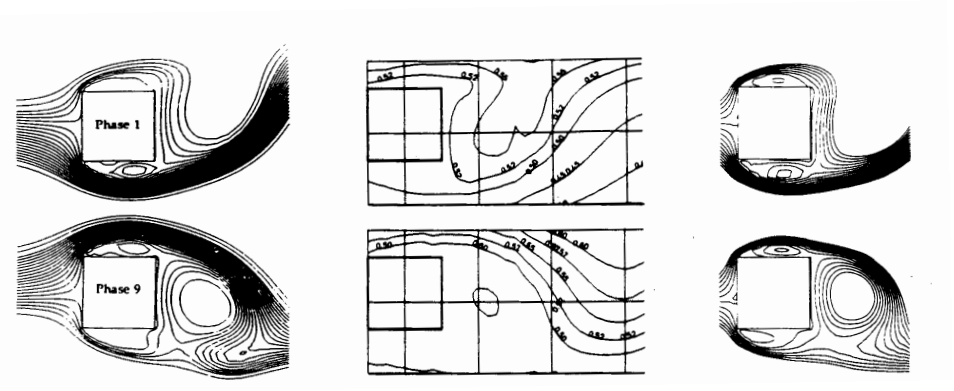


(a) RSE, Experiments, LES

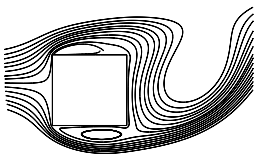

(b) Phase 1, $k-\varepsilon$ + wall laws

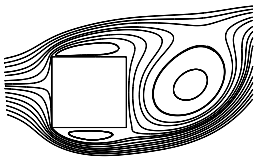

(c) Phase 1, $k-\varepsilon$ + two layers + wall laws

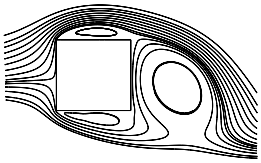

(d) Phase 9, $k-\varepsilon$ + wall laws

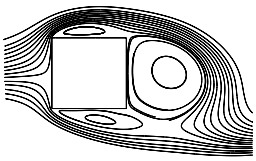

(e) Phase 9, $k-\varepsilon$ + two layers + wall laws

Figure 3: Streamlines for two phases.

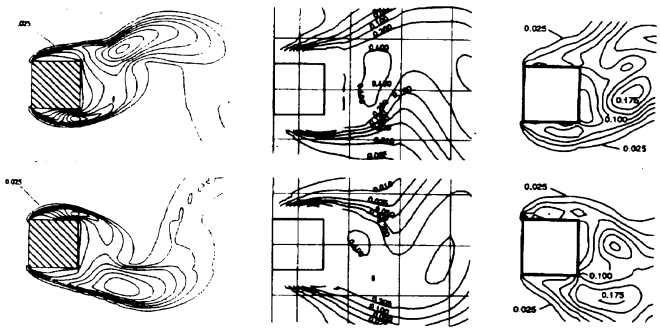

(a) RSE, Experiments, LES

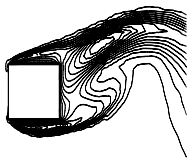

(b) Phase 1, $k - \varepsilon$ + wall laws

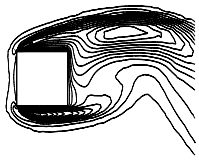

(c) Phase 1, $k - \varepsilon$ + two layers + wall laws

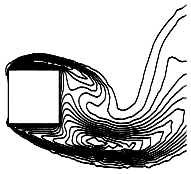

(d) Phase 9, $k - \varepsilon$ + wall laws

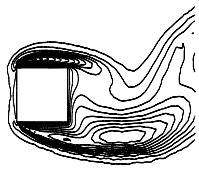

(e) Phase 9, $k - \varepsilon$ + two layers + wall laws

Figure 4: Isolines of $< k >$ for two phases.

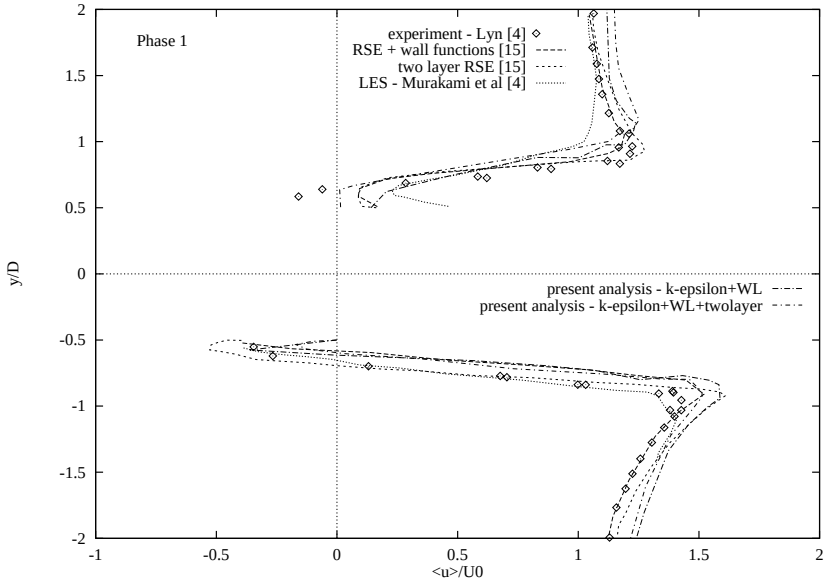


(a) Comparison with experience and other simulations (Phase 1)

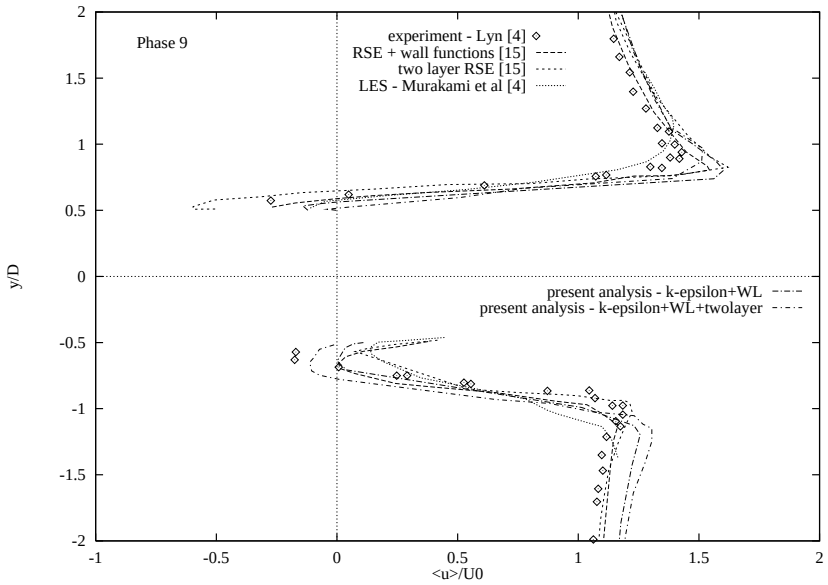


(b) Idem (Phase 9)

Figure 5: Profiles of the mean horizontal velocity component $< u >$ distribution along $x = D/2$ (x-position of the rear cylinder wall).

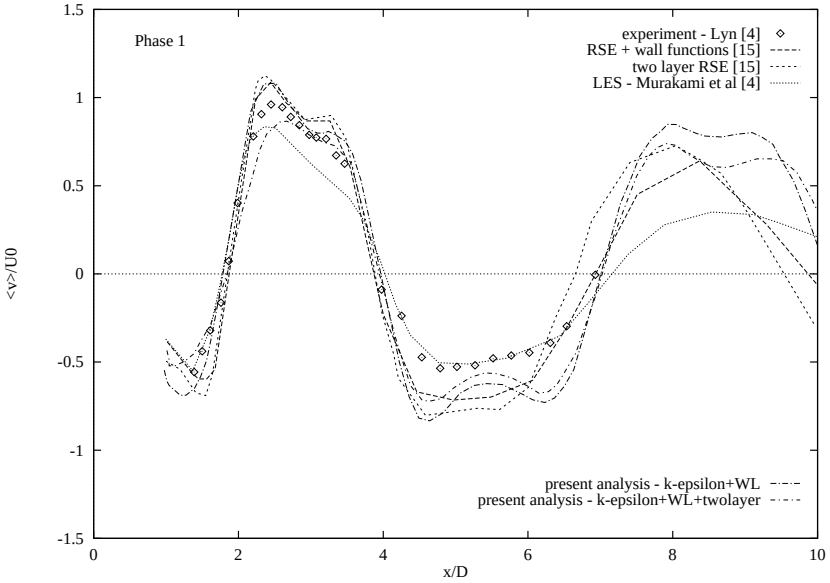


(a) Comparison with experience and other simulations

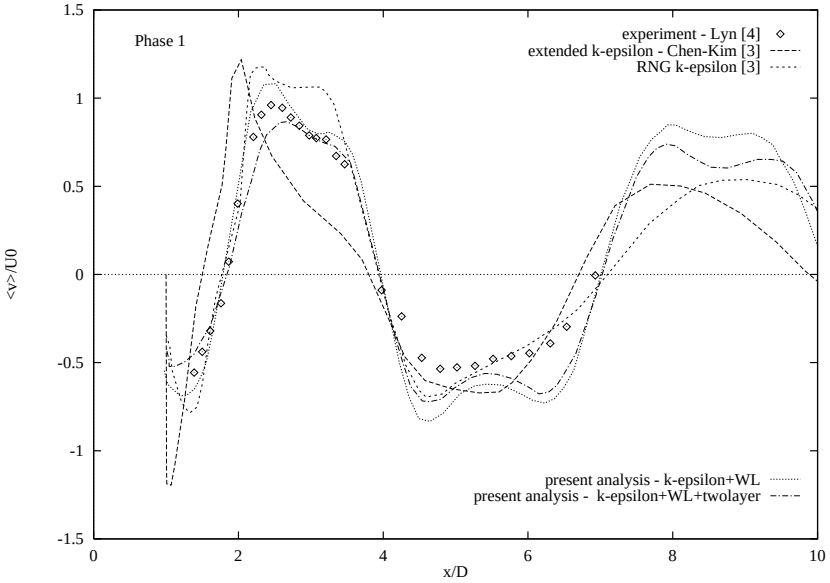


(b) Comparison with other simulations using different $k - \varepsilon$ models

Figure 6: The mean lateral velocity component $< v >$ variation along the centerline (Phase 1).

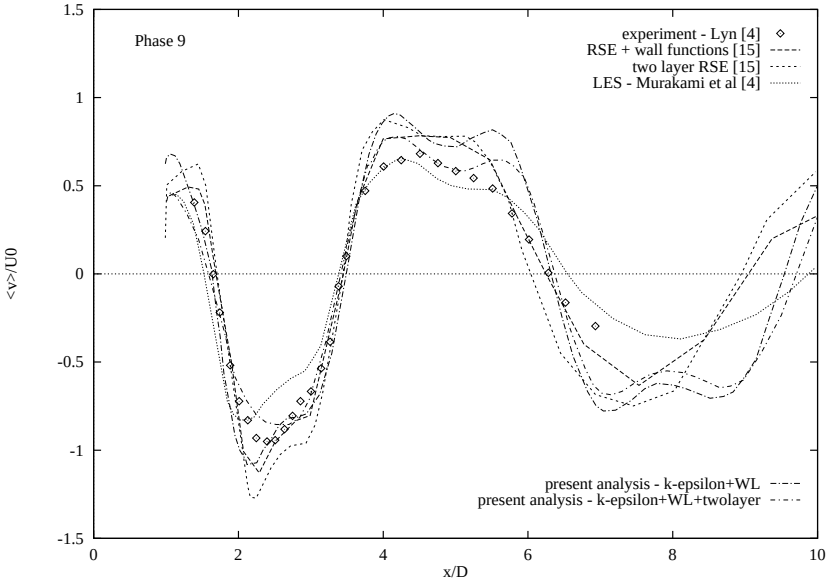


(a) Comparison with experience and other simulations

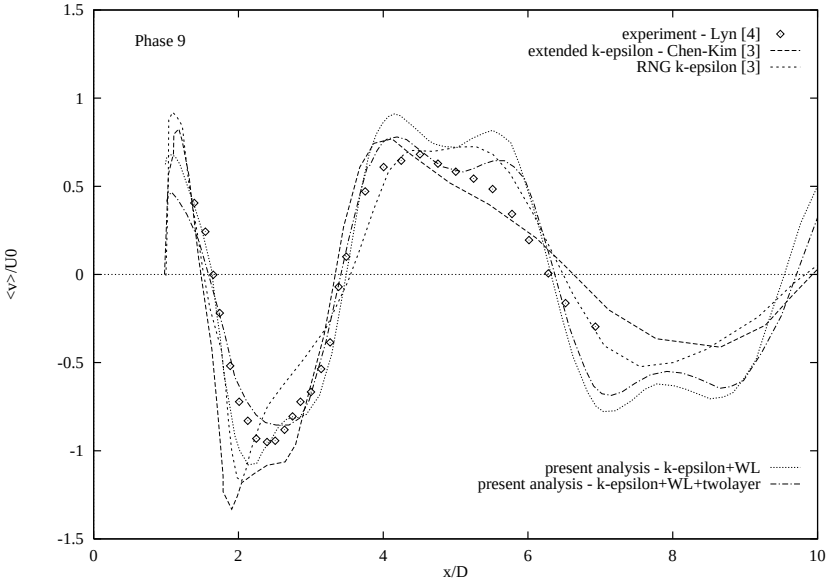


(b) Comparison with other simulations using different $k - \varepsilon$ models

Figure 7: The mean lateral velocity component $< v >$ variation along the centerline (Phase 9).

## 3.2 Flow past a circular cylinder

In this section, the results obtained for the flow past a circular cylinder at various Reynolds numbers are presented. The computations were carried out for Reynolds numbers in the range $Re = 10^4 - 10^6$, including therefore the sub-critical and supercritical regimes and the drag crisis phenomenon.

The results are compared with experimental data obtained by Cantwell and Coles [18] and other simulations presented in [14]. Franke [19] calculated the flow past a circular cylinder at $Re = 1.4 \cdot 10^5$, with both the $k - \varepsilon$ and two-layer RSE models. The general conclusion from that analysis was that the $k - \varepsilon$ model under-predicts the periodic shedding motion, while the RSE model tends to over-predict it, but in the circular cylinder case considerably more than in the square cylinder case. Deng et al (see [14]) calculated the flow past circular cylinders with both the $k - \varepsilon$ model (using various low-Reynolds models near the wall) and the Baldwin-Lomax model. Their conclusion was that all the versions of the $k - \varepsilon$ model underestimate the drag coefficient, but that Baldwin-Lomax gives reasonable results for the global properties. Tamura et al [20] performed both 2D and 3D computations of the flow past circular cylinders with their quasi-LES method (they simulated the effect of smaller-scales turbulent motions by a numerical damping), showing clearly the advantages of a 3D model. In their 2D computations, strong secondary vortices, not present in the 3D computations, caused an over-prediction of the drag coefficient $\bar{c}_D$ in the sub-critical regime. On the other hand, their 3D computations reproduced the behavior of the drag coefficient and in particular its drop with increasing Reynolds number fairly well. Song and Yuan [21] also performed a 2D LES computations that yielded fairly realistic pressure and time-mean velocity distributions for the flow past a circular cylinder at various Reynolds numbers. But they introduced several ad hoc assumptions for this case ([14]).

The starting mesh has about 5000 nodes and is unstructured but symmetric in y. Despite this symmetry, the flow becomes unsteady without any initial perturbation although one could expect the $k - \varepsilon$ not to produce any unsteadiness at all. Three other meshes, obtained after refinement in the normal and tangential directions, have been used. The parameter $\delta$ is set to $(0.001D)$ for the Reynolds number $Re = 10^4$. Here, the impact of several implementation details on the standard $k - \varepsilon$ model is analyzed, keeping in mind the results already obtained for the square cylinder test case:
- the influence of the convection and pressure gradient corrections in the wall laws,
- the influence of the mesh refinement near the wall in normal and tangential,
- the influence of the value of the parameter $\delta$.

The periodic motion has a Strouhal number of $St = 0.26$ for Reynolds number $Re = 10^4$, slightly over-predicting the experimental value of about 0.2 for a wide range of sub-critical Reynolds number values.

The most interesting flow parameter and the most difficult to calculate, is the time-mean drag coefficient. The detailed experimental study of this test case was carried out by Cantwell and Coles [18]. In figure 8, the values of time-mean drag coefficient obtained for various Reynolds numbers in experiments and the data from other simulations are presented. The 3D quasi-LES computations carried out by Tamura et al [20], seem to yield the best agreement with experiences. The results obtained by Deng et al [14] with their Baldwin-Lomax model are also presented. In general, it is reported that the predicted values by the various $k-\varepsilon$ models are not satisfactory.

Similarly to the square cylinder test case, the present analysis yields the values of $\bar{c}_D$ in fairly good agreement with experimental data for the sub-critical regime. For the Reynolds number values that are closer to the critical one (approximately at $5 \cdot 10^5$), the disagreement with the experimental data is more significant. Neither the mesh refinement in tangential and normal directions near the walls, nor the convection and pressure gradient corrections improved these values significantly. The convection and pressure gradient corrections seem to leave some space for improvement as they have been obtained only after a first order expansion [3] and also that the solver is much unstable after their introduction, meaning that improvement in our numerics is still necessary.

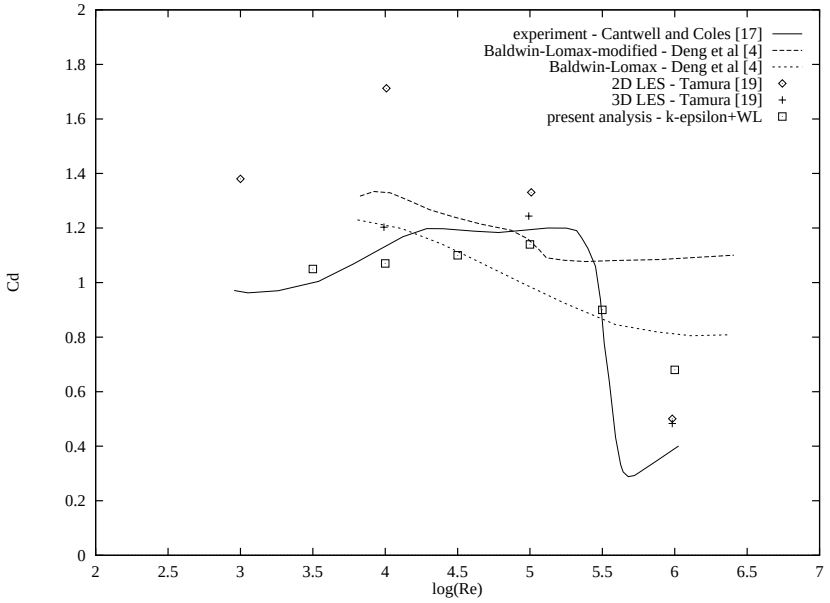


Figure 8: Drag coefficient vs. the Reynolds number.

The results obtained for Reynolds number of $Re = 10^5$ are compared with the results obtained by Franke [19] in his computations using a two-layer $k-\varepsilon$ model and Reynolds stress equations and with the experimental data obtained by Cantwell and Coles for the Reynolds number value $Re = 1.4 \cdot 10^5$.

The length of the separation bubble can be an indicator of the quality of the computations. In figure 9, the predicted instantaneous streamlines at a given phase are presented. We also present the time-mean streamlines obtained by Franke with the two-layer $k-\varepsilon$ model and the two-layer RSE model (we do not produce the time-mean streamlines for our approach as they have been obtained by an a posteriori treatment). We can see that the present approach is quite close to the RSE computations.

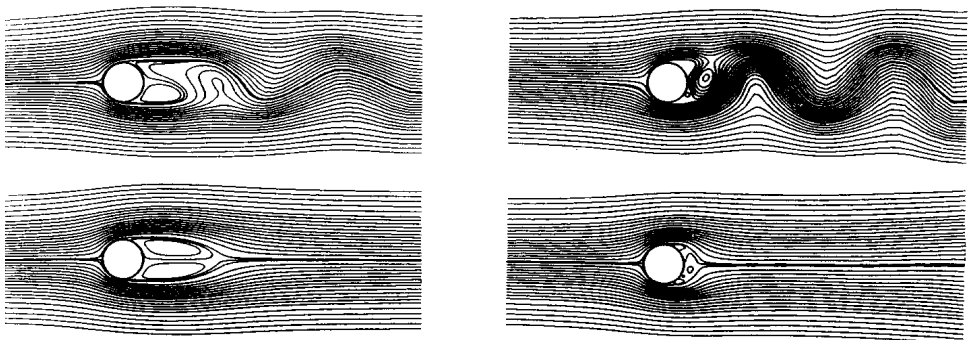

(a) two-layer $k-\varepsilon$ model two-layer RSE model

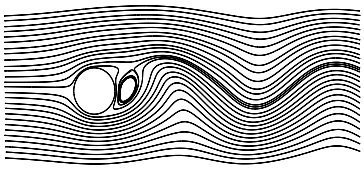

(b) present analysis $k-\varepsilon$ model + wall-laws

Figure 9: Instantaneous streamlines and time-mean streamlines ($Re = 10^5$).

The quality of the results obtained in the vicinity of the cylinder can be evaluated through the values of the time-mean velocity distribution along the center-line behind the circular cylinder. The results from experiments (Cantwell and Coles [18]), Franke's computations [19] and the present analysis are compared in figure 10. It can be seen that none of the computations yield satisfactory results, but the results obtained in the present analysis, again seem to be the best ones. However, there are again some discrepancies in the free-stream velocity approaching region. From the figures 9 and 10, it can be concluded that the model used in the present analysis yields fairly good agreement with the experiments considering the size of the separation region for this Reynolds number value.

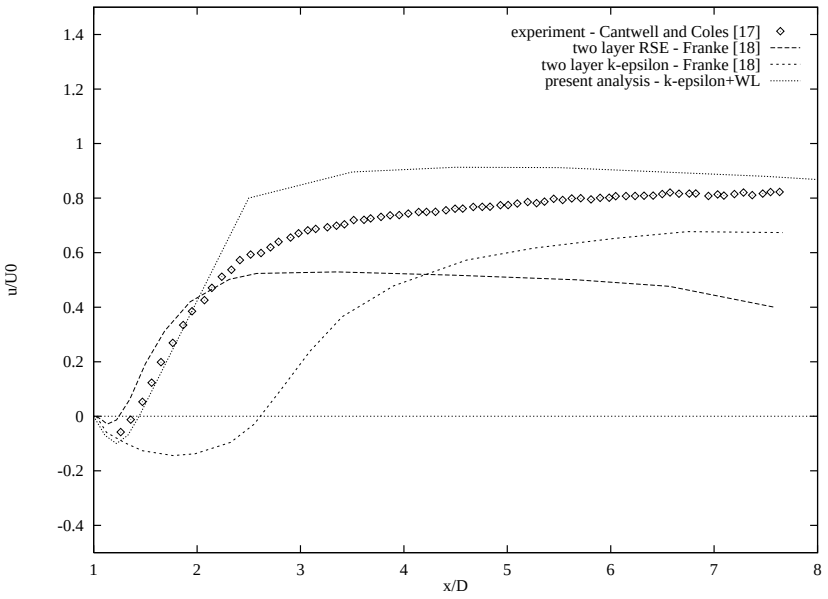


Figure 10: Time-mean horizontal velocity distribution along the center-line behind the circular cylinder ($Re = 10^5$).

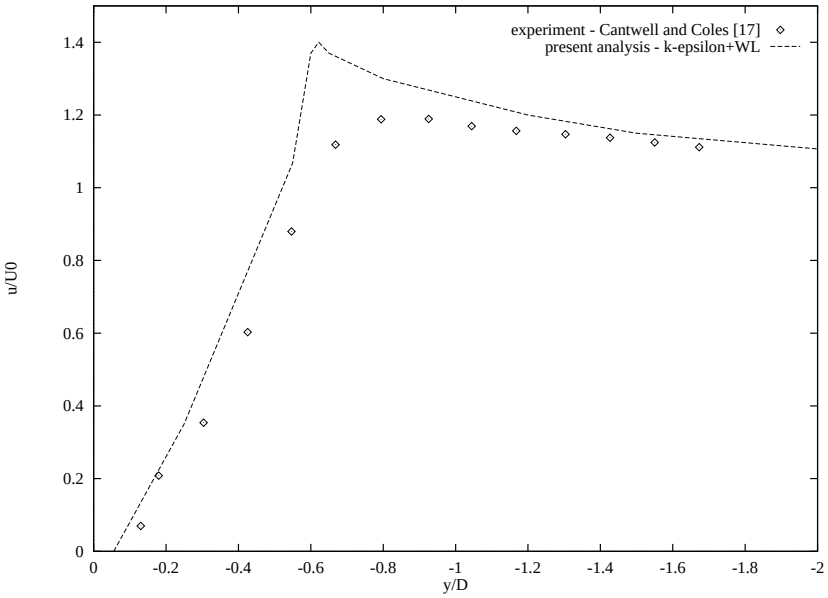


Figure 11: Time-mean horizontal velocity distribution at $x/D = 1$ ($Re = 10^5$).

The time-mean horizontal velocity distribution at $x/D = 1$ obtained in this analysis is compared with experience in figure 11. We can see that, despite being the best, the model over-predicts the horizontal velocity at the boundary of the wake of the cylinder, leading to an unrealistic pressure drop (see figure 12).

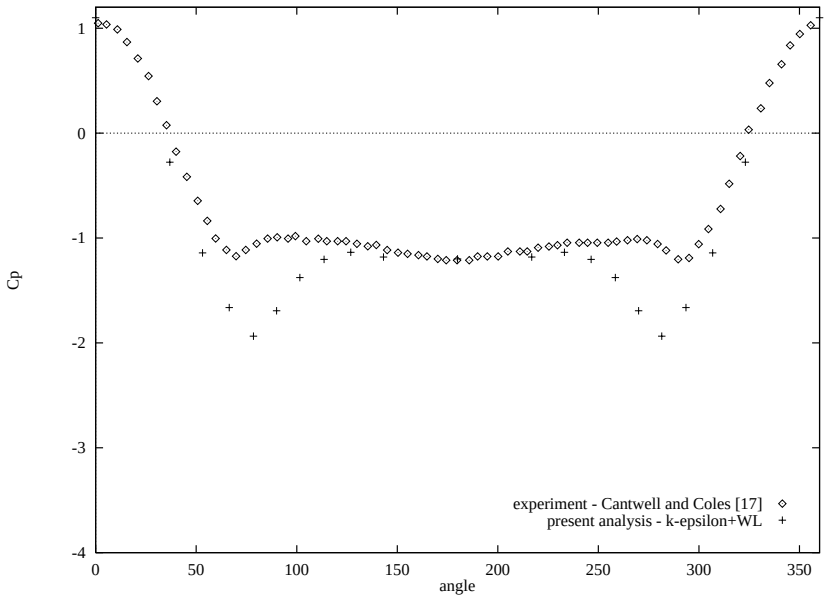


Figure 12: Time-mean pressure distribution on the cylinder surface ($Re = 10^5$).

# 4 Conclusions

Although the classical $k-\varepsilon$ model and wall-laws are expected not to give satisfactory results for unsteady turbulent flows simulations, very good results are obtained with the standard $k-\varepsilon$ model coupled with global wall-laws for two vortex shedding flow problems. The results presented in this paper are in the same quality range than the ones obtained by RSE and LES computations as far as the mean flow remains 2D. Indeed, for the Lyn's test case the agreement is very good as well as for the circular cylinder for Reynolds numbers in the sub-critical range. Failing in the prediction of three dimensional effects in the flow seems therefore to be the major weakness of the model.

In all case we showed that good numerics and adequate numerical dissipation lead to a big improvement of the results obtained with the classical $k-\varepsilon$ model. It is therefore natural to ask the same question for models (like RSE) with much more nonlinearity than $k-\varepsilon$.

# References


[1] B.E. Launder and D.B. Spalding,*Mathematical Models of Turbulence,* Academic Press (1972).

[2] B. Mohammadi and O. Pironneau,*Analysis of the K-Epsilon Turbulence Model*, WILEY, 1994 (Book).

[3] B. Mohammadi and O. Pironneau,*Unsteady Separated Turbulent Flows Computation with Wall-Laws and $k-\varepsilon$ Model,* to appear in CMAME, 1995.

[4] B. Mohammadi,*NSC2KE : an User Guide*, Technical report INRIA No.164, 1994.

[5] G. Comte-Bellot, S. Corrsin,*Simple Eulerian Time-Correlation of Full an d Narrow-Band Velocity Signals in Grid-Generated Isotropic Turbulence,* JFM, vol.48, pp:273-33 7, 1971.

[6] S. Thangam,*Analysis of Two-Equation Turbulence Models for Recirculating Flows*, ICASE report No. 91-61, 1991.

[7] P.L.Roe, *Approximate Riemann Solvers, Parameters Vectors and Difference Schemes,* J.C.P. Vol.43, 1981.

[8] G.D.Van Albada, B. Van Leer,*Flux Vector Splitting and Runge-Kutta Methods for the Euler Equations*, ICASE 84-27, June 1984.

[9] A. Dervieux,*Steady Euler Simulations using Unstructured Meshes*, VKI lecture series, 1884-04, (1985).

[10] R. Struijs, H. Deconinck, P. de Palma, P. Roe, G.G.Powel, *Progree on Multidimensional Upwind Euler Solvers for Unstructured Grids,* AIAA paper 91-1550, (1991).

[11] J. Steger, R.F. Warming, *Flux Vector Splitting for the Inviscid gas dynamic with Applications to Finite-Difference Methods*, J. Comp. Phys. 40, pp:263-293. (1983).

[12] M.H.Lallemand,*Schemas Decentrés Multigrilles pour la Résolution des Equations D'Euler en Eléments Finis*, Thesis, Univ. of Provence-Saint Charles, 1988.

[13] V. Haroutunian and M.S. Engelman,*Two-Equation Simulations of Turbulent Flows: A Commentary on Physical and Numerical Aspects,* ASME 1993 Winter Annual Meeting, New Orleans, USA, 1993.

[14] W. Rodi, *On the Simulation of Turbulent Flow Past Bluff Bodies,* Journal of Wind Engineering and Industrial Aerodynamics, Vol. 46/47, pp:3-19, 1993.

[15] W.Rodi, *LES versus RANS Calculations of Complex Flows past Bluff Bodies,* Proceedings of Basel World CFD Used Days 1996, Third World Conference in Applied CFD, Freiburg, Germany, May 19-23, 1996.

[16] R. Franke and W. Rodi, *Calculation of vortex shedding past a square cylinder with various turbulence models,*, Turbulent Shear Flows 8, Dust et al. (eds.), Springer Verlag, 1993.

[17] G. Bosch, *Experimentelle und theoretische Untersuchung der instationaren Stromungen um zylindrische Strukturen,* Ph.D. Thesis, University of Karlsruhe, 1995.

[18] B. Cantwell and D. Coles, *An experimental study of entrainement and transport in the turbulent near-wake of a circular cylinder,* J. Fluid Mech., Vol. 136, pp.321-374, 1983.

[19] R. Franke, *Numerische berechnung der instationaren Wirbeleblosung hinter zylindrischen Korpern,* Ph.D. Thesis, University of Karlsruhe, 1991.

[20] T. Tamura, I. Ohta and K. Kuwahara, *On the reliability of two-dimensional simulation for unsteady flows around a cylinder-type structure*, J. Wind Eng. and Ind. Aerodyn., Vol. 35, pp. 275-298, 1990.

[21] C.C. Song and M. Yuan, *Simulation of vortex shedding flow about a circular cylinder at high Reynolds numbers,* J. Fluids Eng., Vol. 112, pp. 155-163, 1990.

Unité de recherche INRIA Lorraine, Technopôle de Nancy-Brabois, Campus scientifique,
615 rue du Jardin Botanique, BP 101, 54600 VILLERS LÈS NANCY
Unité de recherche INRIA Rennes, Irisa, Campus universitaire de Beaulieu, 35042 RENNES Cedex
Unité de recherche INRIA Rhône-Alpes, 655, avenue de l'Europe, 38330 MONTBONNOT ST MARTIN
Unité de recherche INRIA Rocquencourt, Domaine de Voluceau, Rocquencourt, BP 105, 78153 LE CHESNAY Cedex
Unité de recherche INRIA Sophia-Antipolis, 2004 route des Lucioles, BP 93, 06902 SOPHIA-ANTIPOLIS Cedex

Éditeur
INRIA, Domaine de Voluceau, Rocquencourt, BP 105, 78153 LE CHESNAY Cedex (France)
ISSN 0249-6399